Tina Memo No. 2006-003
Published in Proc. MIUA 2006
Short version published in Proc. ISMRM 2006

A Simple Electrical Equivalence Model of Intracranial Cerebrospinal Fluid Pulsatility: Design and Validation in Healthy Normals

Jieun Kim, Neil A. Thacker, Paul A. Bromiley, Stephen J. Payne and Alan Jackson

Last updated
10 / 4 / 2006

Imaging Science and Biomedical Engineering Division,
Medical School, University of Manchester,
Stopford Building, Oxford Road,
Manchester, M13 9PT.

A Simple Electrical Equivalence Model of Intracranial Cerebrospinal Fluid Pulsatility: Design and Validation in Healthy Normals

Jieun Kim, Neil A. Thacker, Paul A. Bromiley, Stephen J. Payne and Alan Jackson
Dept. of Medical Biophysics
Imaging Science and Biomedical Engineering Division
Medical School, University of Manchester
Manchester, M13 9PT, UK
neil.thacker@man.ac.uk

Abstract
During the cardiac cycle a complex series of fluid shifts occur within the skull in order to protect the brain from the pressure variations which occur in the cerebral arteries. The extracerebral intracranial arteries dilate during systole generating a pressure wave within the cerebral spinal fluid (CSF). This pressure wave is dissipated by flow of CSF into the compliant spinal subarachnoid space and by direct transmission to the cerebral venous sinuses. This mechanism reduces the pulsatility of the pressure wave to which the brain is exposed during the cardiac cycle. Failure of this mechanism has been implicated in a number of cerebral diseases. The mechanism can be investigated using quantitative magnetic resonance phase imaging but results can be difficult to interpret due to the complexity of the interactions. We present a novel physiological model of this mechanism based on the concept of electrical equivalence. The model allows privation of seven parameters which are not directly measurable: 1) the arterial compliance, 2) brain compliance, 3) ventricular compliance, 4) venous compliance, 5) arterial impedance, 6) brain impedance and 7) impedance of the cerebral aqueduct. We tested the model in a group of 24 healthy normal volunteers. Analysis of individual subjects showed that the data contained in adequate information for reliable fitting. Groupwise analysis showed that the model described all of the statistically significant variation in the data. We conclude that this model forms a basis for the analysis of CSF flow studies although it will require extension if it is to be used to comprehensively describe the abnormalities associated with disease states.

Introduction

In a monograph published in 1783, Alexander Monro a Scottish anatomist applied basic concepts of physics to the contents of the skull [19]. He concluded that 1) the brain was enclosed in a non-expandable case of bone; 2) the substance of the brain was incompressible and consequently that; 3) the volume of blood in the cranial cavity was constant and; 4) that continuous removal of venous blood from the cranial cavity was required to make room for incoming arterial blood. These basic principles were supported in the later work by George Kellie, a former student of Monro, describing experiments in the brains of animals and humans who had died of various causes including hanging and exsanguinations [16]. Later experiments on animals who died by exsanguination reported by John Abercrombie in 1928 also supported the findings of Monroe and Kellie [1] and the doctrine began to attract wide acceptance.

All three of these early workers ignored the existence of cerebral spinal fluid (CSF) and assumed that the volume of intracranial blood was constant, although it could be redistributed between the arterial and venous circulations. This was questioned for the first time in 1846 by George Burrows, an English physician who repeated many of Kellie's experiments on strangulation and exsanguination in rabbits [9]. Burrows concluded that a reciprocal relationship exists between intracranial blood volume and CSF volume and noted that any increase in one required a decrease in the other. It was Cushing who formerly stated the Monro-Kellie hypothesis as it is understood today that: if the skull is intact then the sum of the volume of the brain plus the CSF plus the intracranial blood is a constant [10].

Early applications of the Monro-Kellie hypothesis concentrated on abnormalities which occur in the steady state in diseases such as hydrocephalus and CSF rhinorrhoea [11]. The advent of magnetic resonance imaging (MRI) which provides the ability to non-invasively and quantitatively image CSF and blood flow greatly increased the understanding of CSF dynamics and it has become clear that the constraints of the Monro-Kellie hypothesis result in a complex hydrodynamic mechanism which is required to compensate for the transient increases in cerebral blood volume that occurred during systole [6, 13].

Although the exact effects of the systolic pulse wave within the skull remain the subject of research there is now a general consensus as to the mechanism in normal subjects. Teleologically this mechanism can be seen as a necessary evolutionary development to protect the brain from constant mechanical stresses which would be imposed by repeated systolic expansions of intracerebral vessels by large variations in intraluminal pressure. In normal healthy individuals systolic expansion of the basal arteries occurs proximal to the pial arteriolar resistance vessels responsible for autoregulatory control of cerebral blood flow [4, 13]. Arterial pulsatility produces a pressure wave within the subarachnoid CSF which causes an outflow of CSF through the foramen magnum into the compliant spinal CSF space, equivalent to approximately 50% of the increase in intracerebral blood volume [4]. The pressure wave is also transmitted to the major dural venous sinuses, a mechanism apparently mediated by systolic expansion of the arachnoid granulations [21, 14]. The effect of this is that the energy in the arterial pressure wave entering the cranial cavity is dissipated into the formation of CSF and venous pulsatility and largely bypasses the cerebral circulation. In addition, the elastic properties of expanding arterial walls absorb part of the energy of the systolic pulse wave which is then released in diastole. This has the effect of further flattening the arteriolar pressure profile to which the intracerebral circulation is exposed. Constancy of cerebral perfusion pressure is also maintained by transient systolic increases in venous backpressure within the brain due to direct compression of cortical surface veins by the systolic pulse wave in the subarachnoid CSF space. This combination of processes maintains a constant perfusion pressure and flow in the cerebral capillary bed despite the major pressure changes seen between systole and diastole.

The major importance in the elucidation of these complex autoregulatory mechanisms is the increasing recognition that they are deranged in a wide range of cerebral diseases. This has led to a reappraisal of the pathogenetic mechanisms behind a wide range of diseases including communicating hydrocephalus [13] normal pressure hydrocephalus (NPH) [6, 3], idiopathic intracranial hypertension (IIH) [5, 17], secondary intracranial hypertension (SIH) [5], the ischaemic white matter change known as leukoaraiosis (LA) [4], neurodegenerative and mixed dementias and other cerebral atrophic disorders [2, 20]. For example: modern theories of hydrocephalus identify a chronic form of communicating hydrocephalus which is believed to result from decreased compliance in basal arteries which gives rise to break down of the windkessel mechanism causing increased pulsatility in cerebral arterioles and capillaries. This causes an intermittent trans-mantle pressure differential leading to progressive ventricular dilation until a new physiological balance is reached [13]. Many other pathogenetic mechanisms mediated by a breakdown in this autoregulatory system have been postulated including decreased arteriolar resistance with a resultant increase in cerebral blood flow (IIH) [17], increased venous resistance due to partial outflow of destruction (SIH) [5], focal reductions in venular compliance (LA) [4], and reduced venous compliance due to abnormally large transmission of the systolic CSF pressure wave to the venous sinuses causing superficial cortical vein compression (NPH) [6].

The generic problem with these studies is their reliance on varying sets of phenomenological observations which are potentially open to alternate interpretations. For example: we have recently described increased transmission of the systolic pulse wave into the cerebral capillaries in elderly patients with treatment resistant depression [20]. This was demonstrated by a decrease in the latency between arteriolar and cerebral aqueductal systole and an increase in cerebral pulsatility indicated by aqueductal flow volume. We have interpreted this as an epiphenomenon of, and potential biomarker for the decrease in arteriolar compliance associated with microvascular angiopathy (cerebral small vessel atheroma). However, several alternative interpretations are possible, for example: the increasing brain pulsatility could reflect a change in the compliance of the brain substance (due to ischaemic white matter changes) in the presence of a normal vascular pulse pressure. The complexity of this autoregulatory process, the variations in measurements and interpretation methods recommended by different groups [13, 3, 18, 15, 5, 22] and the limitations on the number of measurements which can be obtained (due to the capability of MR flow techniques and the imaging time required in individual subjects) combine to make such phenomenological observations increasingly unsatisfactory.

There is a clear need for a quantitative model of the mechanism to act as a substrate for principled analysis of this type of data. Such a model should: 1) allow direct comparison between different study designs; 2) enable the identification of pathogenetic abnormalities interfering with this autoregulatory mechanism which would not be susceptible to simple phenomenological observation and 3) allow testing and validation of specific data driven analysis techniques to identify minimum required data sets to support valid conclusions regarding clinical diagnosis and pathogenetic mechanisms in specific disease processes.

A full modelling approach would involve a finite element model for a given individual based upon the Navier-Stokes equations, including viscosity terms and elastic tissue boundaries. This would require a level of detailed knowledge relating to tissue structure and its properties that is unrealistic for practical application. However, an analysis of the physical modelling process leads us to conclude that many aspects of such systems can be described by a limited (and therefore measurable) set of effective parameters describing grouped anatomical regions. This raises the possibility of realistic models with practical utility.

In this paper we construct a bulk parameter model based upon an analogy to an electrical circuit, treating the impedance of flow paths as resistances and the compliance of thin boundaries as capacitances. We then evaluate the model using MRI data obtained from young healthy control subjects. The analogy used to model the biological system as an electrical circuit is shown in Fig 1. Previous workers have described similar electrical equivalent models of intracranial hydrodynamics and have tested them with simulated data sets [23, 24]. However, this paper represents the first evaluation of such an electrical equivalent model using measured data from living subjects.

Materials and Methods

Underlying Anatomical Model

In order to construct an equivalent electrical model it is important to define the anatomical model which it will represent. A series of underlying assumptions are implicit in the construction of any model based system. Throughout this study we have applied assumptions and data selection criteria based on findings of previous studies. The basic model (shown in Fig 1) assumes that:

1. The model applies only to the changes taking place within a rigid skull cavity Rigid skull

2. There is pulsatile flow of blood into the skull through the arteries, through the brain into the venous system and then out of the skull.

3. The arterial system lies largely within the subarachnoid CSF space.

4. The venous system lies largely within the subarachnoid CSF space.

5. The brain lies within the subarachnoid CSF space and contains a CSF cavity representing the ventricular system.

6. That the ventricles communicate with the subarachnoid CSF space through a restricted opening.

7. That the subarachnoid CSF space communicates with the spinal CSF space.

8. That the spinal CSF space is compliant.

Our implementation of the model and analysis of the data further assumes that:

1. The measured arterial inflow of obtained by combining measurements from the carotid and basilar arteries represents the absolute cerebral blood flow within the model,

2. That the measured CSF flow through the Foramen Magnum represents the absolute CSF flux between the intracranial and spinal CSF spaces

3. That the measured cerebral aqueductal CSF flow represents the absolute CSF flux between the ventricular system and subarachnoid CSF space.

We believe that it is important to specifically state these assumptions since we anticipate that the model we will describe will require extension and modification in order to support its application in disease states. The reasons and justification for this deliberate oversimplification are discussed in detail below.

Electric Equivalent CSF Pulsatility Model

We assume that we can represent all time varying signals in the Fourier domain so that we can analyse the equivalent circuit at a fixed set of frequencies w. We can then analyse this circuit using conventional means by specifying current flows and deriving equations describing current and voltage.

Since the rate of CSF production is small compared to the flows occurring during the cardiac cycle, we would expect all mechanisms relating to net production of CSF to be either negligible or approximately linear within a single cardiac cycle, and thus have no effect on any non-zero frequency Fourier terms. Only the first half of the Fourier terms are necessary for the model as the rest are constrained in order to have the zero imaginary terms required for a physical system.

Assuming fixed values for compliances and impedances within this system we can write down an equivalent model as an electrical circuit (Fig (a)). Flow paths with impedance are modelled as resistors and elastic surfaces between any two pressure reservoirs (arteries, brain, veins, CSF, ventricles and spine) are modelled as capacitors. Some of the components are redundant (cannot be constrained with the available measurements) and must be combined to produce a simplified circuit (Fig 2(b)). This system has 11 free parameters ((R_1 - R_5, C_1 - C_5 and V_3) and 6

possible measurements (I_1 - I_4 and V_1 - V_2). Such a combination of parameters, whilst necessary, complicates the biological interpretation of the parameters in the simplified model.

Analysis of Current Flows

The application of Kirchoff's laws to the circuit shown in Fig 2(b) leads to the following equations:

Vertex Currents

$$I_1 = I_5 + I_6 \tag{1}$$
$$I_8 = I_9 + I_2 \tag{2}$$
$$I_6 = I_3 + I_7 + I_8 \tag{3}$$
$$I_4 = I_5 + I_3 + I_7 + I_9 \tag{4}$$

Voltage loops

$$I_5 R_5 + I_5 \frac{1}{jwC_1} - I_3 R_2 - I_3 \frac{1}{jwC_2} - I_6 R_1 = 0 \tag{5}$$

$$I_7 \frac{1}{jwC_3} - I_9 \frac{1}{jwC_4} - I_8 R_3 = 0 \tag{6}$$

$$I_3 \frac{1}{jwC_2} + I_3 R_2 - I_7 \frac{1}{jwC_3} = 0 \tag{7}$$

Point to point voltages

$$V_2 - V_1 = I_6 R_1 + I_8 R_3 + I_2 R_4 \tag{8}$$
$$V_3 - V_1 = I_6 R_1 + I_3 \frac{1}{jwC_2} + I_3 R_2 + I_4 \frac{1}{jwC_5}. \tag{9}$$

We have introduced 5 new current variables (I_5 to I_9), and we have 9 equations, leaving 6 degrees of freedom. The point-to-point voltages require the equivalent of pressure measurements in the biological system. The unmeasured current variables from the seven remaining constraint equations must be eliminated, leaving two equations composed of variables which are either measured or are compliance and impedance parameters of the biological system.

After eliminating unwanted variables (see Appendix for detail), we have obtained three important equations to note: the Monro-Kellie hypothesis Eq. 10, which is simply a statement of volume preservation; the constraint equation Eq. 11 relating currents, which does not contain I_1, C_5 or R_4; and Eq. 12, which scales the variables using mean potentials.

$$I_1 = I_2 + I_4 \tag{10}$$

Box 1: Monro-Kellie Principle.

$$(R_5 + D_{1w} + R_1)[I_3(D_{2w} + R_2)(D_{3w} + D_{4w} + R_3) - D_{3w}(I_4 - I_3)D_{4w} - D_{3w}(I_4 - I_3 + I_2)R_3]$$
$$+ D_{3w}[I_3(R_2 + D_{2w}) + (I_2 + I_4)R_1](R_3 + D_{4w}) = 0 \tag{11}$$

Box 2: Constraint equation relating currents (flows).

$$< V_3 > - < V_1 > = < I_1 > R_1 \tag{12}$$

Box 3: Using mean potentials (pressures) to scale variables.

Parameter Estimation

A likelihood-based approach was adopted in order to estimate the parameters of the model. We can build a suitable likelihood function from Eq. 11. Substituting Eq. 10 and re-organising terms, we obtain an equation of the form

$$\gamma I_3 \; - \; \alpha I_1 \; + \; \beta I_4 \; = \; 0 \tag{13}$$

where α, β and γ are complex variables given as;

$$\alpha \; = \; wC_2[C_1R_1 \; - \; C_4R_3 \; - \; jC_1C_4R_3R_5]$$

$$\beta \; = \; C_2(wC_1(R_1 \; + \; R_5) \; - \; j)$$

$$\gamma \; = \; j(C_1 \; + \; C_2 \; + \; C_3 \; + \; C_4)$$

$$-w[C_2R_2(C_3 \; + \; C_4) \; + \; C_4R_3(C_2 \; + \; C_3) \; + \; C_1((R_1 \; + \; R_5)(C_3 \; + \; C_4) \; + \; C_2(R_1 \; + \; R_5 \; + \; R_2) \; + \; C_4R_3)]$$

$$- \; jw^2[C_1C_2(R_1 \; + \; R_5)R_2(C_3 \; + \; C_4) \; + \; C_4R_3(C_1(R_1 \; + \; R_5)(C_2 \; + \; C_3) \; + \; C_2R_2(C_1 \; + \; C_3))]$$

$$+ \; w^3C_1C_2C_3C_4(R_1 \; + \; R_5)R_2R_3.$$

The above equations define the noise-free constraint. Applying the variational method to the constraint equation Eq. 13, the complex residual on the constraint for each Fourier amplitude w in the measured currents is;

$$F_w \; = \; \gamma I_{3w} \; - \; \alpha I_{1w} \; + \; \beta I_{4w}.$$

We then obtain the inverse likelihood to be minimised in the form of a sum over the appropriate Mahalanobis distance terms from each measured frequency w;

$$-log(P) \; = \; \sum_w F_w^* F_w / var(F_w) \tag{14}$$

where the variance on the complex residual is given by

$$var(F_w) \; = \; \alpha^* \alpha \; \sigma_1^2 \; + \; \beta^* \beta \; \sigma_4^2 \; + \; \gamma^* \gamma \; \sigma_3^2$$

Box 4: Optimisation Function.

Having determined the most likely parameters for the model we can now make corrections to the flow variables ΔI_n in order to enforce the constraint equations, in a way which minimises the change in the measurements consistent with the measurement errors:

$$\chi^2 \; = \; \sum_w \Delta I_1^* \Delta I_1 / \sigma_1^2 \; + \; \Delta I_3^* \Delta I_3 / \sigma_3^2 \; + \; \Delta I_4^* \Delta I_4 / \sigma_4^2.$$

The minimum of this function at fixed frequency, consistent with the flow constraints (Substitute for I_1, differentiate with respect to I_3 and I_4, set the resulting equations to zero and solve them) is given by:

$$\Delta I_1 \; = \; \frac{\alpha^* F \; \sigma_1^2}{\alpha^* \alpha \; \sigma_1^2 \; + \; \beta^* \beta \; \sigma_4^2 \; + \; \gamma^* \gamma \; \sigma_3^2}$$

$$\Delta I_3 \; = \; \frac{-\gamma^* F \; \sigma_3^2}{\alpha^* \alpha \; \sigma_1^2 \; + \; \beta^* \beta \; \sigma_4^2 \; + \; \gamma^* \gamma \; \sigma_3^2}$$

$$\Delta I_4 \; = \; \frac{-\beta^* F \; \sigma_4^2}{\alpha^* \alpha \; \sigma_1^2 \; + \; \beta^* \beta \; \sigma_4^2 \; + \; \gamma^* \gamma \; \sigma_3^2}$$

The substitution of these equations into the expression for χ^2 above regenerates the earlier expression for $-log(P)$ in Eq. 14. This demonstrates that the parameter estimation process is a direct minimisation of these residual functions.

Subjects and MR Image Acquisition

MR image volumes were acquired from 24 healthy control subjects (18 male with average age 35 and 6 female with average age 24). Written informed consent was obtained from all subjects. Sagittal T1-weighted images and phase-contrast angiography scout images were acquired to identify the acquisition plane, which was perpendicular to the flow (Fig 3 (a) and (b)). Velocity encoded PC-cine MR images were acquired of CSF flow velocity at the cerebral aqueduct (AQ) and foramen magnum (FM), and arterial blood flow velocity in the basilar artery (BA) and both internal carotid arteries (CA). Retrospective cardiac gating using vector electrocardiography (VECG) was used to generate 16 images spanning the cardiac cycle for each subject. All subjects were scanned using a 3T Philips Medical Systems whole body scanner with a multi-element head coil. The image parameters were: flip angle 10-15; 5-7mm slice thickness; TR (repetition time) 8.82 - 22.13 ms; and TE (echo time) 8.14 - 14.39 ms; V_{enc} (velocity encoding) was set at 10cm/sec for the for AQ and FM, and 90cm/sec for the BA and CA. Scan time was usually 2-4 min for each region and total scanning time was 15-30min including scout imaging, depending mainly on the subject's heart rate.

Typical images at a single time point for each region are shown in Fig 3 (1-5). High intensity values represent systolic flows, and low values represent diastolic flows. AQ and FM sequences contain both systolic and diastolic flows: BA and CA sequences contain only systolic positive flow images.

In five patients the measurements were repeated in order to assess measurement reproducibility. Since it is the precision of the measurement which will affect the errors generated within the model subjects were scanned without removal from the scanner or any other intervention taking place between the two imaging sets.

Image processing

In order to obtain a reliable estimation of the flow, a quadratic function was fitted over the region of the cerebral aqueduct at each time point in the cardiac cycle. An approximate location for the centre of the aqueduct was provided manually and a 3x3 region was fitted for all subjects. The area under this curve was then integrated for all values of the function.

The BA and CA flows were estimated from the sum of flow values within the region of the arteries, defined by thresholding the modulus images to find the region of interest (ROI), as shown in Fig 3. Total flow through the carotid and basilar arteries (CAB) was then calculated by combining the measured values. The flow into the FM was obtained in the same way as the BA flow. Typical flow curves obtained from the MR images are shown in Fig 4. Note that the FM flow closely follows the CA and BA flow and the peak delay between CA and BA flow and AQ flow.

Results

Given measured AQ flow (I_3), FM flow (I_4), and CAB flow (I1), Eq. 14 can be minimised as a function of the remaining parameters (R_2, R_3, R_5, C_1 - C_4). The estimated flows I_3 and I_4 can be corrected back to zero mean. The ratio of R1:R3 was fixed at 4:1 in order to reduce the number of degrees of freedom in the model, because the greater part of the pressure drop is known to occur in the arterial vessels and the fraction 4:1 is an estimate of the relevant proportions based on previous measurements [8]. We then normalised all remaining parameters to R_1.

Given the compliances (C_i) and impedances (R_i) of the system and the arterial blood flow and cerebral aqueduct flow, all other flows can be computed starting from Eq. 13 and working back through the other results. The model can thus be used in a forward manner in order to determine the effects of parameter changes on flow and pressure curves.

Typical input curves and error corrected model output flow curves for one subject are shown in Fig 5(a)-(c). Flow measurements in the reproducibility study of 5 subjects suggested that the errors on the measured curves are of the order of 0.114 ml/sec for the foramen magnum, 0.174 ml/sec for the arteries and 0.00114 ml/sec for the cerebral aqueduct. These errors were used to scale the Fourier terms in Eq. 11. The corrected flow curves (Fig 5(a)-(c)) are consistent within the expected error on the measurement, which implies that the model is adequate to describe the data.

Model Parameter Estimation

Initially, an attempt was made to fit the model parameters using data from individual subjects. Figure 8 shows a typical set of optimised model parameters. Figure 5 (d) shows the computed flow values at all other points in the model for one specific individual. Of particular interest are the curves for I_6 and I_8, the flows through intermediate-sized blood vessels within the brain. These curves are essentially flat within the expected error, demonstrating that almost all pulsatility has been removed from the arterial input curves, as expected in a normal brain. This appears to be due to shunting of the pulsatile component for the arterial input through the foramen magnum. The measured arterial input and foramen magnum curves are similar in shape. This implies that in this individual most of pulsatility of arterial flow passes through I5 and then through CSF space, and the bulk flow is through I_6 and I_8.

However, for 17 of the 24 control subjects parameters R_2, R_3 and C_1 did not return a well-determined minimum. In addition, the fits for 8 of the 24 subjects returned trivial solutions in which the C_3 and C_4 parameters converged to zero. We took this to indicate that, in many individual cases, the data did not contain enough significant Fourier terms to allow accurate estimates of the unconstrained fitting.

Since fitting the model to individual subjects proved unreliable, a second phase of fitting was conducted, in which a group-wise approach was adopted. A sub-set of the data was selected, consisting of the 16 subjects who gave non-trivial solutions in terms of the C_3 and C_4 parameters for individual fits. The model parameters were then optimised simultaneously across this data group. This approach was based on the assumption that the physical parameters of the model do not vary greatly between normal individuals. Therefore, variations between individuals were implicitly assumed to represent differences in systemic behaviour. Thus, the group-wise approach provided additional information on the typical range of model parameters for normal subjects which further constrained the fitting process. The optimised parameters, normalised to R_1, are shown in Fig 6. The χ^2 has 762 degrees-of-freedom (16 measurements of 3 flow curves for 16 subjects, minus the 6 degrees-of-freedom of the model) and so gives a χ^2 per degree-of-freedom of 1.9 at the optimum. The good agreement of the model and data as shown in Fig 5 (a) (c) suggests that the reproducibility analysis slightly underestimated the measurement errors. The optimum parameters are given numerically in Table 1. The errors shown are the standard errors of the model fit. The very small value returned for the elastic capacity of the capillaries, C_3, would seem to imply that this parameter is redundant, as would be expected on the basis of observations in normal subjects.

Once the model had been optimised in this group-wise fashion, it was retrospectively applied to the 8 data sets omitted from the parameter optimisation. In 7 of these subjects, the model described all of the statistically significant variation in the data (i.e. produced a χ^2 per degree-of-freedom consistent with that obtained in the fitting process). The flow curves for the single remaining data set, which was not consistent with the group model, are shown in Fig 7.

Conclusions and Discussion

In this work, we have attempted to concatenate and refine the features of the electrical circuit models presented previously in the literature, and to validate the resultant model using flow data obtained from MR images of 24 normal subjects. In comparison to previous work, some CSF production mechanisms, such as production from arteries (Fig 9 diode/resistor coupling I) have been removed since their effects are expected to be negligible within a cardiac cycle [23, 24]. The other major difference between the model presented here and the well known Ursino model is the introduction of ventricular and extra-cerebral compliances. The Ursino model uses the equivalent of the spinal compliance in our model to describe intracranial compliance [23, 24]. However, being earthed on one side, it has the physical analogy of being set in a vacuum, thus preventing the presence of a non-zero mean pressure in the brain. The original authors compensated for this by the use of a "mock CSF injection rate" (Fig 9 current generator at e [23]), which is not needed in our model.

The results from fitting the refined model to individual subjects indicated that, even with a markedly simplified anatomical model, the information content of the data is too low to provide stable estimates of the model parameters in the majority of cases. Therefore, a group-wise approach was adopted, in which the model parameters were optimised simultaneously over those data sets that returned non-trivial solutions for individual model fits. This procedure succeeded in producing a stable set of optimised parameters. Retrospective application of this optimised model to the data sets omitted from the group-wise fitting showed that, in all but one of the subjects, the model described all of the statistically significant variation in the data. This confirms that the difficulty encountered in fitting the model to individual data sets is related to the information content of the data, rather than an inability of the model to describe the whole range of normal variation. We therefore conclude that the optimised model provides a valid description of the pulsatile flow within the cranium in normal subjects. The failure of the model

to fit in one individual case is most likely to represent anatomical or physiological variation within this individual which has not been specifically accounted for within the simplified model. The implications of oversimplification of the model are discussed in detail below.

The simplified model allows quantitative derivations of seven parameters: 1) the arterial compliance, 2) brain compliance, 3) ventricular compliance, 4) venous compliance, 5) arterial impedance, 6) brain impedance and 7) impedance of the cerebral aqueduct. However, these seven parameters can only be measured up to a scale factor using Eq. 11 so we must select one and fix it to a nominal value. In order to estimate absolute values of the 7 estimated parameters it would be necessary to directly measure two pressures (arterial venous or CSF) within the system for each individual. Even under these circumstances it would be important to realise that the equivalence between compliance and capacitance is not straightforward. Compliance is the equivalence of permittivity, not capacitance, and to obtain compliance (the measure of tissue elasticity) would require scaling variables such as cross-sectional areas and volumes, which is impracticable at this time.

The model presented here is based on the simplest possible anatomical interpretation of the system and represents the simplest electrical equivalence model that can be specified. Consequently, for some parameters, particularly the resistances, it is difficult to precisely identify the equivalent anatomy. This represents a very deliberate oversimplification and it is important to understand the rationale on which this was based since it impacts directly on the further development of the model and the applications to which it can be applied. The initial consideration in the design of the current model was the extremely limited number of physical measurements that could be acquired in order to drive the fitting process. We have assumed that flow measurements in the arterial inflow, cerebral aqueduct and foramen magnum correctly represented absolute measurements of fluid flux over the cardiac cycle. In normal individuals, where collateral vascular circulation does not exist and CSF flow through the fourth ventricle is at low pressure these are justifiable assumptions. Although it is technically straightforward to apply quantitative flow measurements through the cerebral venous system we have specifically excluded venous flow measurements from fitting process. This decision was made on the basis of the extreme variability of the superficial cortical venous drainage system which has been reported by several workers [5, 7, 12]. It is clear that measurements from individual cerebral veins and major dural venous sinuses cannot be considered to represent the absolute venous outflow from any specific part of the brain. Previous work have assumed that the pulse waves observed in the major dural venous sinuses are a true representation of the pulsatility patterns seen in the overall venous outflow from the system. However, there is little or no evidence to support this assumption and the extreme variability of venous anatomy and venous flow patterns cast significant doubt on the validity of such an assumption. Furthermore, Eq. 10 indicates that, once any two of arterial flow, venous flow, and flow through the foramen magnum have been measured, measurement of the third does not help to constrain the model parameters.

It is clear that the inability of the model to reliably fit to data from individual subjects limits the applicability of the model in its current incarnation, even though this failure reflects a paucity in the data content rather than a failure of the model. Furthermore, a critical review of the literature concerning CSF pulsatility indicates that the model will be over-simplistic if it is applied to pathological conditions. Firstly, there is a clear functional dichotomy between the superficial and deep cerebral venous drainage territories in the way that they respond in different disease states [6, 3]. Secondly, there is a need to understand the distribution of systolic pulse wave energy within the superficial venous system and major dural venous sinuses in order to allow the model to account for anatomical variations in superficial cortical drainage and, thirdly, it is possible that the restriction of CSF flow at the tentorial incisura may require explicit modelling of supra and infra tentorial flow mechanisms.

This is most likely to be the case where CSF abnormalities result primarily from disorders within the posterior fossa such as the Arnold-Chiari malformation or posterior fossa mass lesions.

The next essential step in the development of the model is therefore to identify additional measurable inputs which could be used to drive the fitting process. In principle phase contrast flow measurements could be extracted from a range of other anatomical locations. Measurement of flow through the tentorial incisura may allow separate modelling of supra-tentorial and infra-tentorial compartments but would require significant extension of the model which is unlikely to be supported by the relatively small amount of additional data provided. More importantly, it is possible to measure pulsatile venous flow at other sites in the venous system including the straight sinus, sigmoid and transverse sinuses, extracerebral jugular vein and major superficial cortical veins such as the Great Vein of Labbe which represent the principal collateral venous flow mechanism from the prosencephalic cortex. Predictions of specific components of venous outflow derived from the existing model could be compared to observed measurements in order to extend the model to include central venous and collateral superficial venous drainage pathways. Although this model would be more complex, it would also be closer to clinical applicability and fitting process would be supported by the ability to include additional measured venous output parameters.

In summary we have developed a simple electrical equivalence model which describes the interactions between intracranial arterial and CSF flow patterns observed in normal individuals. This is the first time that a model of

this type has been tested with genuine data. The model allows direct proportional (but not absolute) estimation of seven parameters which cannot be derived by direct measurement. These are: 1) the arterial compliance, 2) brain compliance, 3) ventricular compliance, 4) venous compliance, 5) arterial impedance, 6) brain impedance and 7) impedance of the cerebral aqueduct. Although the model is deliberately simplistic, it allows for potential extension to allow for more sophisticated description of anatomical and pathological variations. We conclude 1) that the model presented here provides a valid description of the interaction between into cerebral blood flow and CSF movements and 2) the model be used to support is to allow inclusion of additional anatomical and pathological variation which will be required to support its application in disease states.

Acknowledgements

Authors would like to thank Dr. Marietta Scott for her helpful comments and Mr. Barry Whitnall for his role in scanning and collecting MR data.

Appendix

Elimination of Unwanted Variables

This section describes in detail the elimination of unwanted variables used to produce a set of irreducible equations. First, eliminate I_8 using Eq. 2 from Eqs. 3 and 6;

$$I_6 \;=\; I_3 \;+\; I_7 \;+\; I_9 \;+\; I_2 \tag{15}$$

$$I_7\frac{1}{jwC_3} \;-\; I_9\frac{1}{jwC_4} \;-\; (I_9 \;+\; I_2)R_3 \;=\; 0. \tag{16}$$

Eliminate I_6 using Eq. 15 from Eqs.1 and 5

$$I_1 \;=\; I_5 \;+ I_3 \;+\; I_7 \;+\; I_9 \;+\; I_2 \tag{17}$$

$$I_5R_5 \;+\; I_5\frac{1}{jwC_1} \;-\; I_3(R_2 + \frac{1}{jwC_2}) \;-\; (I_3 \;+\; I_7 \;+\; I_9 \;+\; I_2)R_1 \;=\; 0. \tag{18}$$

Eliminate I_9 using Eq. 17 from Eqs. 15, 16 and 18;

$$I_1 \;=\; I_2 \;+\; I_4 \tag{19}$$

Box 1: Monro-Kellie Principle.

This equation is entirely in terms of measured data and is therefore irreducible.

$$I_7\frac{1}{jwC_3} \;-\; (I_4 \;-\; I_5 \;-\; I_3 \;-\; I_7)\frac{1}{jwC_4} \;-\; (I_4 \;-\; I_5 \;-\; I_3 \;-\; I_7 \;+\; I_2)R_3 \;=\; 0 \tag{20}$$

$$I_5R_5 \;+\; I_5\frac{1}{jwC_1} \;-\; I_3(R_2 + \frac{1}{jwC_2}) \;-\; (I_2 \;+\; I_4 \;-\; I_5)R_1 \;=\; 0. \tag{21}$$

Eliminate I_7 using Eq. 7 from Eqs. 20 and 21;

$$I_7 \;=\; jwC_3I_3(\frac{1}{jwC_2} \;+\; R_2) \tag{22}$$

giving

$$I_7(\frac{1}{jwC_3} \;+\; \frac{1}{jwC_4} \;+\; R_3) \;-\; (I_4 \;-\; I_5 \;-\; I_3\;)\frac{1}{jwC_4} \;-\; (I_4 \;-\; I_5 \;-\; I_3 \;+\; I_2)R_3 \;=\; 0 \tag{23}$$

$$jwC_3I_3(\frac{1}{jwC_2} \;+\; R_2)(\frac{1}{jwC_3} \;+\; \frac{1}{jwC_4} \;+\; R_3) \;-\; (I_4 \;-\; I_5 \;-\; I_3)\frac{1}{jwC_4} \;-\; (I_4 \;-\; I_5 \;-\; I_3 \;+\; I_2)R_3 \;=\; 0. \tag{24}$$

Finally rewrite Eq. 21 in terms of I_5 and use this in Eq. 24 to produce the final irreducible equation.

$$I_5 \;=\; \frac{I_3(R_2 + \frac{1}{jwC_2}) \;+\; (I_2 \;+\; I_4)R_1}{\frac{1}{jwC_1} + R_1 + R_5} \tag{25}$$

Use $\frac{1}{jwC_n} \;=\; D_{nw}$ as shorthand so that all R's are real and all D's imaginary (all I's are complex);

$$(R_5 + D_{1w} + R_1)[I_3(D_{2w} + R_2)(D_{3w} + D_{4w} + R_3) - D_{3w}(I_4 - I_3)D_{4w} - D_{3w}(I_4 - I_3 + I_2)R_3]$$
$$+ D_{3w}[I_3(R_2 + D_{2w}) + (I_2 + I_4)R_1](R_3 + D_{4w}) = 0 \quad (26)$$

Box 2: Constraint equation relating currents (flows).

Notice that this equation does not contain I_1, C_5 or R_4 (though I_1 can be re-introduced using Eq. 20). Thus this equation cannot be used to determine these parameters. In addition there is an overall unknown scale factor leaving a total of 6 degrees of freedom. This constraint equation is complex and therefore provides two constraints for non-zero frequencies. The zeroth order term yields just one equation for the case of $< I_3 > = < I_4 > = 0$ (i.e. no net flow out of the ventricles and into the spine) with $< I_2 > \neq 0$ and $D_{3w} \neq 0$.

Using the equations relating point-to-point voltages

Scaling of the parameters requires the use of a point-to-point voltage equation (such as Eq. 8 or Eq. 9). In fact an alternative point-to-point voltage route gives a simple measurable form immediately.

$$V_3 - V_1 = I_5 \frac{1}{jwC_1} + I_4 \frac{1}{jwC_5}$$

Substituting in Eq. 25 and Eq. 19 while introducing our shorthand gives

$$V_3 - V_1 = \frac{I_3(R_2 + D_{2w}) + I_1 R_1}{D_{1w} + R_1} D_{1w} + I_4 D_{5w}. \quad (27)$$

which, again for the mean flow case and $< I_3 > = < I_4 > = 0$ reduces to

$$< V_3 > - < V_1 > = < I_1 > R_1 \quad (28)$$

Box 3: Using mean potentials (pressures) to scale variables.

This suggests that the scaling factor for R_1 (and therefore all of the parameters) can be determined from the zeroth order term. Higher order terms (requiring Fourier terms of $V_1(t)$) provide a constraint on parameter C_5, but do not require additional temporal measurement of V_3, which has been assumed to be static.

References

1. J Abercrombie J *Pathological and practical researches on disease of the brain and spinal cord.* Edinburgh, 1828.
2. G A Bateman. Pulse wave encephalopathy: a spectrum hypothesis incorporating Alzheimer's disease, vascular dementia and normal pressure hydrocephalus. *Med Hypotheses* 62(2):182-7, 2004.
3. G A Bateman. The reversibility of reduced cortical vein compliance in normal pressure hydrocephalus following shunt insertion. *Neuroradiology* 45:65-70, 2003.
4. G A Bateman. Pulse-wave encephalopathy: a comparative study of the hydrodynamics of leukoaraiosis and normal-pressure hydrocephalus. *Neuroradiology* 44(9):740-8, 2002.
5. G A Bateman. Vascular hydraulics associated with idiopathic and secondary intracranial hypertension. *AJNR Am J Neuroradiol* 23(7):1180-6, 2002.
6. G A Bateman. Vascular Compliance in Normal Pressure Hydrocephalus. *AJNR Am J Neuroradiology* 21: 1574-1585, 2000.
7. S C Beards, S Yule and A Jackson. Anatomical variation of cerebral venous drainage: the theoretical effect on jugular bulb blood samples. *Anaesthesia* 53(7):627-33, 1998.
8. R M Berne and M N LevY. *Caridiovascular Physiology.* London: Mosby, 2001.
9. G Burrows.(1848) *On disorders of the cerebral circulation and on the connection between affections of the brain and diseases of the heart.* Philadelphia: Lea & Blanchard, 1848.
10. H Cushing. *The third circulation in studies in intracranial physiology and surgery.* London: Oxford University Press, 151, 1926.
11. W P Dillon and R A Fishman. Some lessons learned about the diagnosis and treatment of spontaneous intracranial hypotension. *AJNR Am J Neuroradiol* 19(6):1001-2, 1998.
12. P Gideon, C Thomsen, P S Sorensen, F Stahlberg and O Henriksen. Measurement of blood flow in the superior sagittal sinus in healthy volunteers, and in patients with normal pressure hydrocephalus and idiopathic intracranial hypertension with phase-contrast cine MR imaging. *Acta Radiol* 37(2): 171-6, 1996.
13. D Greitz. Radiological assessment of hydrocephalus: new theories and implications for therapy. *Neurosurg Rev* 2004;27(3): 145-165, 2004.
14. D Greitz, T Greitz, T Hindmarsh. A new view on the CSF-circulation with the potential for pharmacological treatment of childhood hydrocephalus. *Acta Paediatr* 86(2): 125-32, 1997.
15. V B Joseph, L Raghuram, I P Korah and A G Chacko. MR ventriculography for the study of CSF flow. *AJNR Am J Neuroradiol* 24(3): 373-81, 2003.
16. G Kellie. Appearances observed in the dissection of two individuals; death from cold and congestion of the brain. *Trans Med-Chir Soc Edinburgh* 1: 84, 1824.
17. N T Mathew, J S Meyer and E O Ott. Increased cerebral blood volume in benign intracranial hypertension. *Neurology* 25(7) 646-9,1975.
18. T Miyati, M Mase, T Banno, T Kasuga, K Yamada, H Fujita, K Koshida, S Sanada and M Onoguchi. Frequency analyses of CSF flow on cine MRI in normal pressure hydrocephalus. *Eur Radiol*2003;13:1019-1024, 2003.
19. A Monro (1783) *Observations on structure and functions of the nervous system.* Edinburgh: Creech and Johnson, 1783.
20. J Naish, R C Baldwin, T Patankar, S Jeffries, A S Burns, C J Taylor, J C Waterton and A Jackson A. Abnormalities of CSF flow patterns in the cerebral aqueduct in treatment resistant late life depression: a potential biomarker of microvascular angiopathy. *MRM. Mag Reson Med*, 2006 (Submitted).
21. E Stolz, M Kaps, A Kern, S S Babacan, W Dorndorf. Transcranial color-coded duplex sonography of intracranial veins and sinuses in adults. Reference data from 130 volunteers. *Stroke* 30(5) 1070-5, 1999.
22. C Strik, U Klose, M Erb, H Strik and W Grodd. Intracranial oscillations of cerebrospinal fluid and blood flows: analysis with magnetic resonance imaging. *J Magn Reson Imaging* 15(3) 251-8, 2002.
23. M Ursino and C A Lodi. A simple mathematical model of the interaction between intracranial pressure and cerebral hemodynamics. *J Appl Physiol* 82(4) 1256-69, 1997.
24. M Ursino and C A Lodi. Interaction among autoregulation, CO2 reactivity, and intracranial pressure: a mathematical model. *Am J Physiol* 274(5 Pt 2) H1715-28, 1998.

Table 1: Fitted parameters from entire data set (arbitrary units).

Parameter	Physical interpretation	Value	Standard error
R_1	impedance of arterial capillaries	1.0	0.025
R_2	impedance of cerebral aqueduct	≈ 0.0	-
R_3	impedance of venous capillaries	≈ 0.0	-
R_5	impedance of arteries	0.01	8×1.8^{-3}
C_1	elastic capacitance of arteries	$\approx$large	-
C_2	elastic capacitance of ventricles	4.11	0.11
C_3	elastic capacitance of capillaries	≈ 0.0	5×10^{-3}
C_4	elastic capacitance of veins	271.017	18

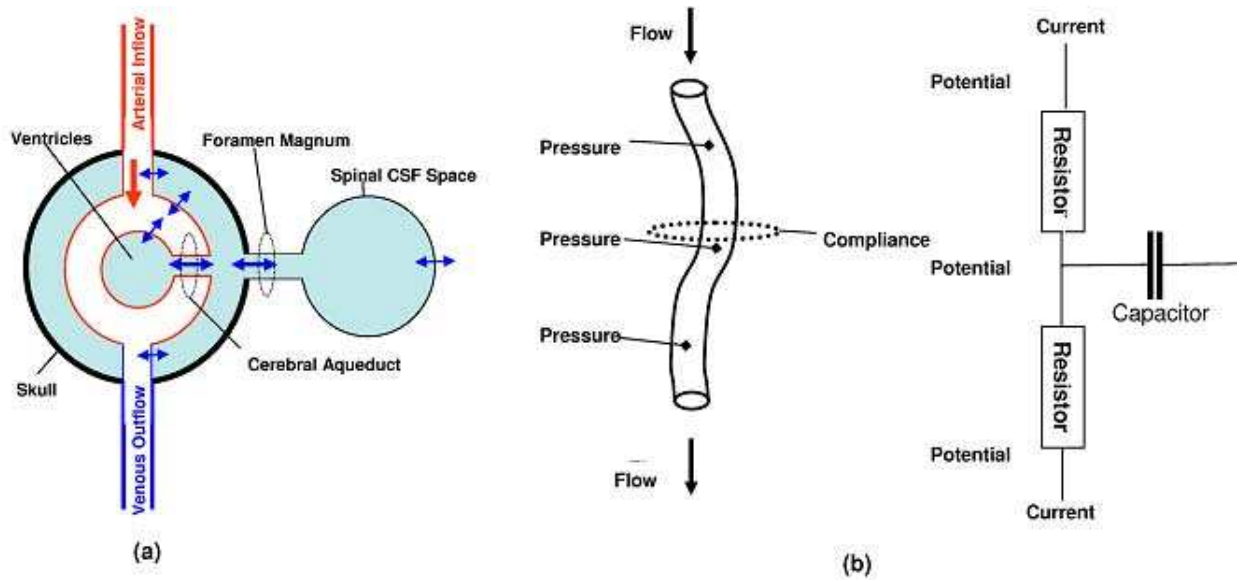

Figure 1: Biological system and electric current. **(a)** Simplified anatomical model on which the electrical equivalence model is based. Narrow flow paths are expected to have associated impedances and thin boundaries are expected to have compliances which can transmit influence of pressure between fluid pools. **(b)** Analogy between current and flow. Both systems can be characterised by analogous 1st order differential equations.

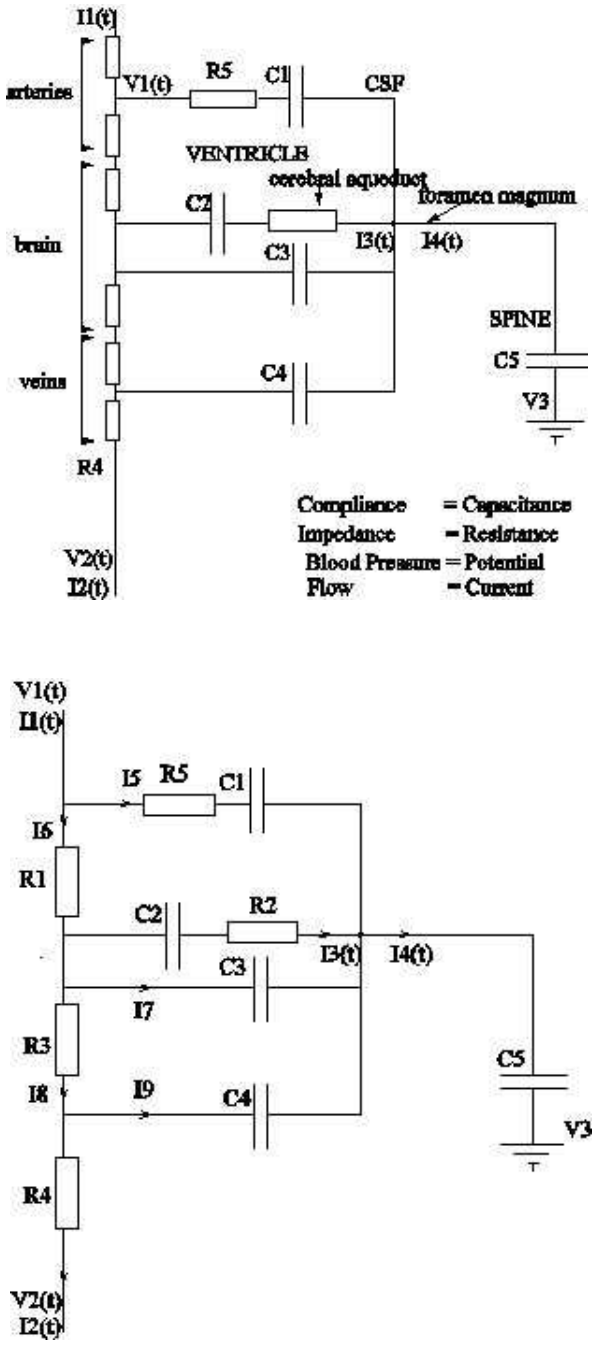

Figure 2: Electrical Circuits for the simplified biological model. **(a)** Analogous electrical circuit. **(b)** Combination of redundant components and specification of all current path variables.

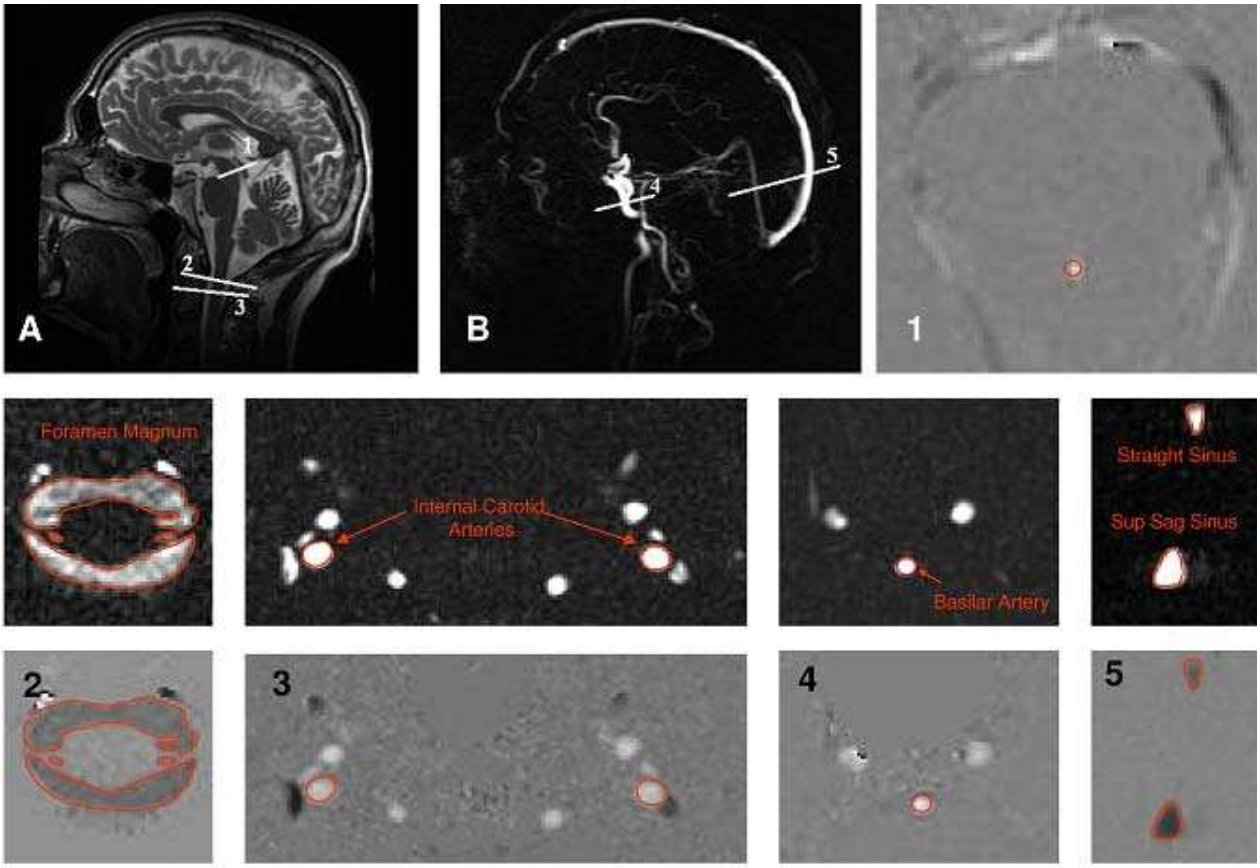

Figure 3: MR images. **(a)** Sagittal T1 scout image used to determine flow acquisition level and oblique axis for 1-AQ, 2-CA, 3-FM. **(b)** Phase contrast angiogram used to determine flow acquisition level for 4-BA, 5-SS. **1-5** Typical velocity encoded MR images of the vessels in which flows were measured. **1** AQ **2** FM **3** CA **4** BA **5** SS. The middle row shows corresponding modulus images

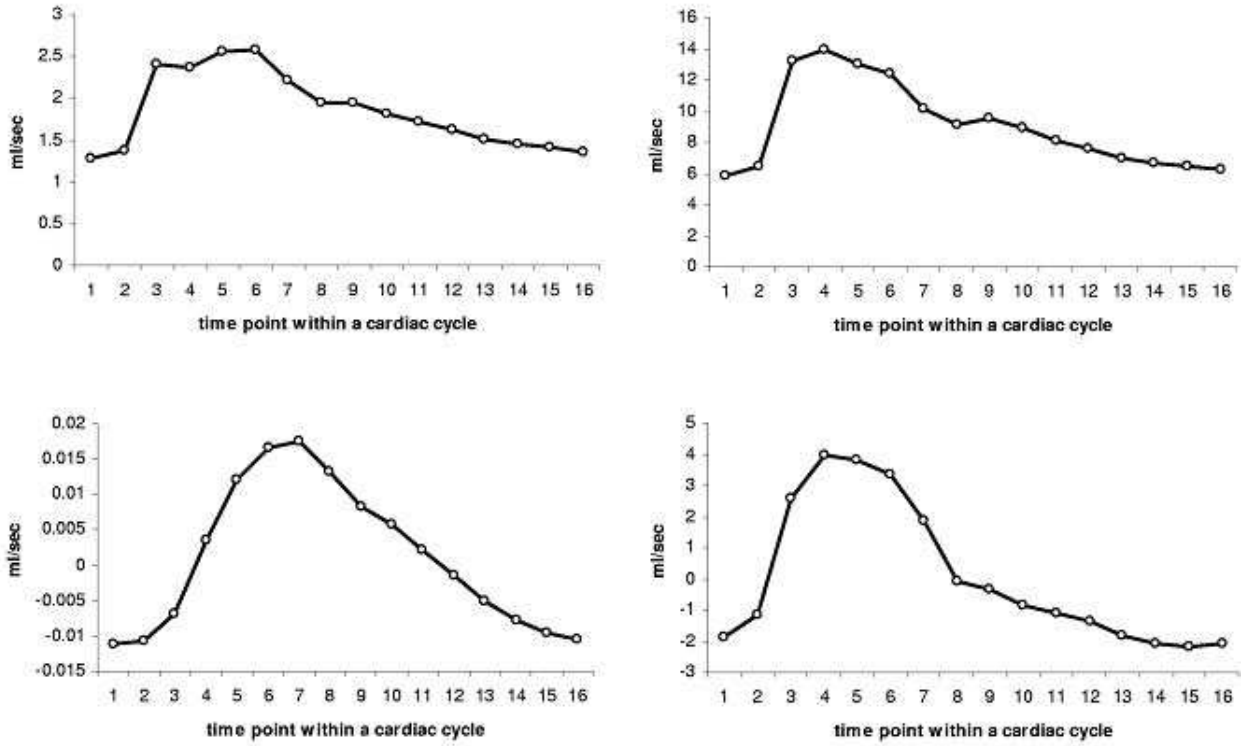

Figure 4: Typical flow rate results. The abscissa shows 16 time points within one cardiac cycle. **(a)** flow at BA **(b)** flow at CA **(c)** flow at AQ **(d)** flow at FM.

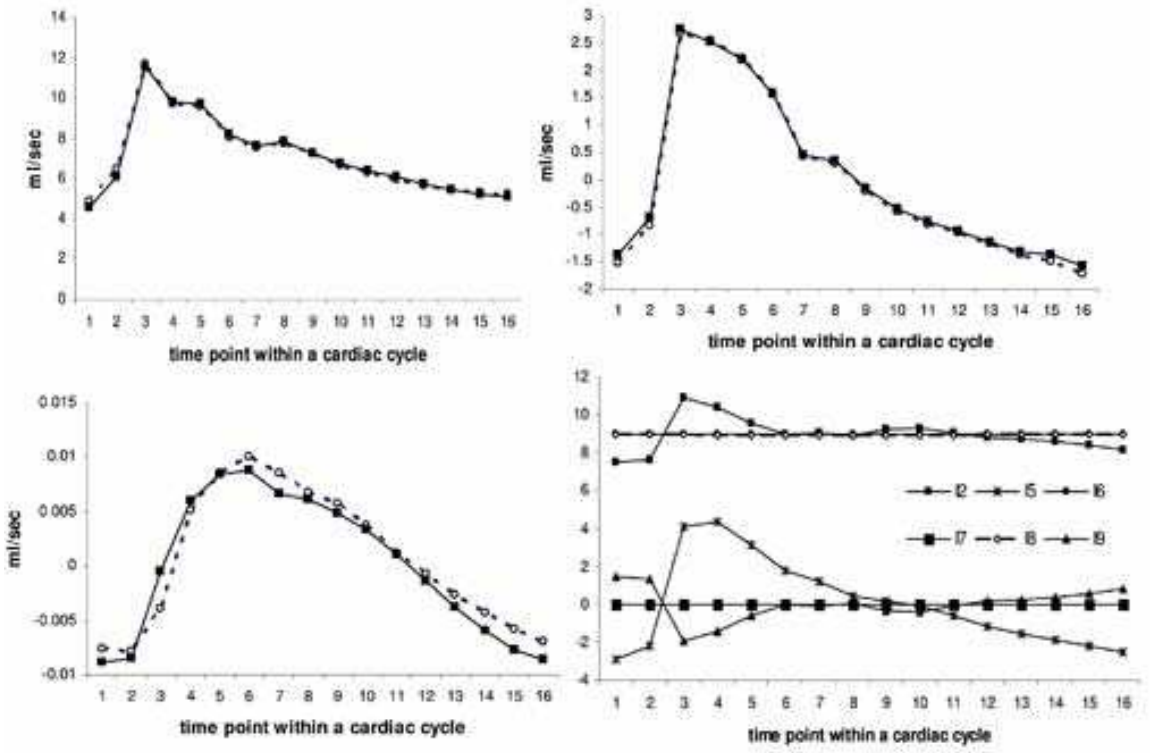

Figure 5: MR flow measurements (input to the model) and estimated error-corrected flow output for one individual from the model at **(a)** CAB, **(b)** FM, **(c)** AQ, **(d)** shows the remaining flow output from the model.

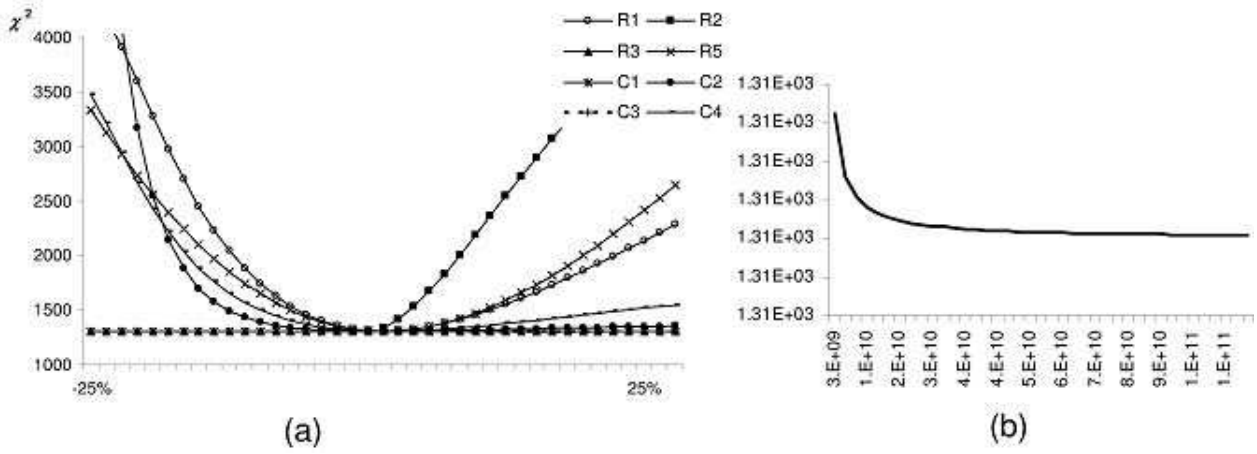

Figure 6: χ^2 values for fitted parameters for the entire group: R_3 is not included because we have fixed a ratio R_1:R_3=4:1. The χ^2 has 762 degrees-of-freedom. **(a)** the abscissa is given as a percentage variation of the optimal parameter value. **(b)** shows the parameter fitting of C_1, where the abscissa is given as the actual parameter value.

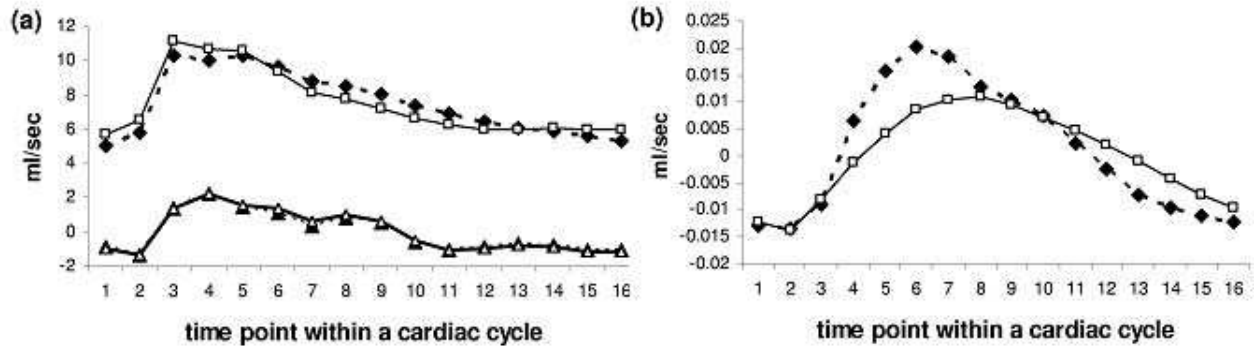

Figure 7: Flow curves from the individual not well described by the groupwise model. **(a)** CAB and FM. **(b)** AQ.

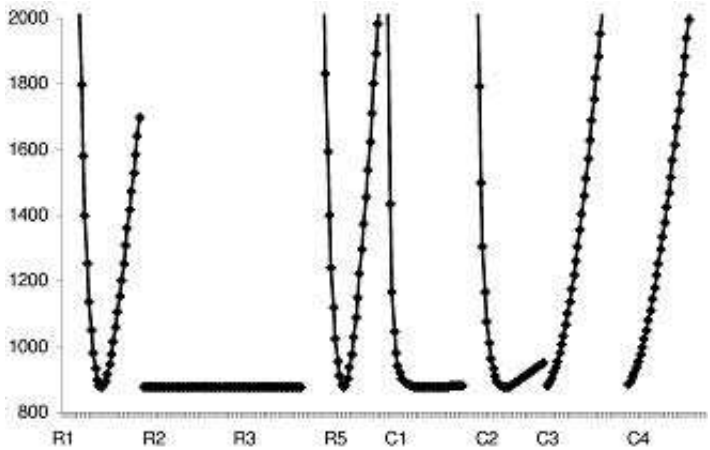

Figure 8: A typical set of optimised model parameter from individual subjects.

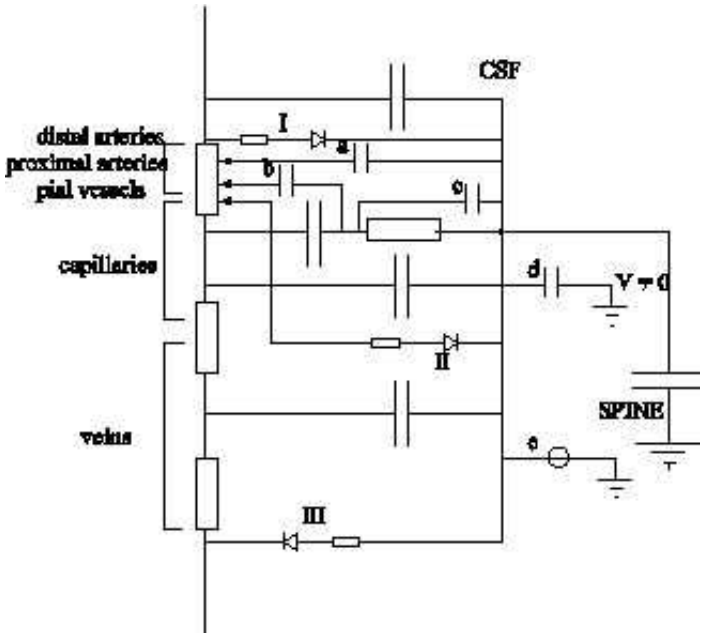

Figure 9: Full electrical circuit. As many specific parts of the anatomy as possible are identified as separate parameters.